

Analyst

Accepted Manuscript



This is an *Accepted Manuscript*, which has been through the Royal Society of Chemistry peer review process and has been accepted for publication.

Accepted Manuscripts are published online shortly after acceptance, before technical editing, formatting and proof reading. Using this free service, authors can make their results available to the community, in citable form, before we publish the edited article. We will replace this *Accepted Manuscript* with the edited and formatted *Advance Article* as soon as it is available.

You can find more information about *Accepted Manuscripts* in the [Information for Authors](#).

Please note that technical editing may introduce minor changes to the text and/or graphics, which may alter content. The journal's standard [Terms & Conditions](#) and the [Ethical guidelines](#) still apply. In no event shall the Royal Society of Chemistry be held responsible for any errors or omissions in this *Accepted Manuscript* or any consequences arising from the use of any information it contains.

Hierarchically Assembled NiCo@SiO₂@Ag Magnetic Core-Shell Microspheres as Highly Efficient and Recyclable 3D SERS Substrates

Maofeng Zhang^{a,b}, Aiwu Zhao^{a,b*}, Dapeng Wang^a, Henghui Sun^a

a. Institute of Intelligent Machines, Chinese Academy of Sciences, Hefei, 230031, P. R. China

b. State Key Laboratory of Transducer Technology, Chinese Academy of Sciences, Hefei, 230031, P. R. China

* Corresponding author: E-mail: awzhao@iim.ac.cn

Abstract

The hierarchically nanosheet-assembled NiCo@SiO₂@Ag (NSA) core-shell microspheres have been synthesized by a layer-by-layer procedure at ambient temperature. The mean particle size of NSA microspheres is about 1.7 μm , which is made up of some nanosheets with an average thickness of ~ 20 nm. The outer silver shell surface structures can be controlled well by adjusting the concentration of Ag⁺ ions and the reaction times. The obtained NSA 3D micro/nano structures show a structure enhanced SERS performance, which can be attributed to the special nanoscale configuration with wedge-shaped surface architecture. We find that NSA microspheres with nanosheet-assembled shell structure exhibit the highest enhancement efficiency and high SERS sensitivity to p-ATP and MBA molecules. We show that the detection limits for both p-ATP and MBA of the optimized NSA microspheres substrates can approach 10^{-7} M. And the relative standard deviation of the Raman peak maximum of $\sim 13\%$, which indicates its good uniformity of the substrate. In addition, the magnetic NSA microspheres with high saturation magnetization show a quick magnetic response, good recoverability and recyclability. Therefore, such NSA microspheres may have great practical potential applications in rapid and reproducible trace detection of chemical, biological and environment pollutants with a simple portable Raman instrument.

Keywords: NiCo, Ag, microsphere, magnetic, SERS

1. Introduction

Surface-enhanced Raman scattering (SERS) spectroscopy have given birth to a powerful and versatile novel analytical tool due to its high sensitivity, specificity, and fingerprint effect in the detection of analytes,¹⁻⁴ thus has tremendous potential for chemical and biomolecular sensing and identification.^{5,6} The enormous SERS enhancement effect enables this technique for trace or even single molecule level detection of a variety of molecules, including proteins,⁷ anthrax,⁸ DNA,⁹ explosives,¹⁰ environmental contaminants,¹¹ and so on. Recently, three-dimensional (3D) Ag and Au micro/nanostructures, (such as flower-like,¹² sea urchin-like,^{13,14} star-like,¹⁵ sphere-like,¹⁶ as well as dendritic morphologies¹⁷), which contain special fine structure, large specific surface area, and larger size, have stimulated great interest recently for several obvious advantages and their excellent performance as SERS substrates. Both experimental measurements and theoretical calculations have proven that strong electromagnetic field enhancement can be produced between adjacent nanostructures on the surface of the 3D complex structures.¹⁸⁻²⁰ To date, various kinds of 3D Ag and Au micro/nanostructures have been successively synthesized and reported. Despite these amazing advances, it must be emphasized that most of these SERS substrate are thrown away after once detection probably because they can not be recycled. This would result in a waste of the resources which usually are made of noble metal (Au or Ag). From the application viewpoint, it is of considerable importance to develop an efficient SERS substrate that can not only provide strong enhancement factors, but also show high stability and reproducibility.

The combination of noble metals and magnetic materials as SERS substrates has been proved to be an effective way of solving the problem described above. Magnetic-based noble metals composites can be recycled, economic, and their function can be recovered by several washing. In particular, the combination of plasmonic and magnetic materials in a single micro/nanostructure is of high interest to the biomedical community because it has the potential to lead to new biological applications, such as immunomagnetic separation under plasmonic imaging monitoring, dual mode imaging (MRI and plasmonic imaging), and SERS sensing. For example, yang *et al* had demonstrated the synthesis of Ag-coated Fe₃O₄ microsphere as a SERS substrate holding clean and reproducible properties under an external magnetic force;²¹ Also, they showed a facile one-step solvothermal method to the synthesis of sea-urchin-like Fe₃O₄@C@Ag particles, which can be used as a SERS substrate possessing reproducible properties;²² Wang *et al* reported a well-dispersed Fe₃O₄@SiO₂@Ag with a nanosheet assembled shell structure exhibiting good reproducibility across the entire area;²³ Recently, our group has developed Fe₃O₄@C@Au composite microspheres with superior SERS detection and recyclable catalytic degradation abilities for organic dyes.²⁴ The above mentioned magnetic core-shell materials generally employ Fe₃O₄ as a magnetic core, while metals and alloys materials (such as Fe, Co, Ni, FePt, and FePd) are less commonly employed as magnetic cores,²⁵ in part because of their rapid oxidation in air

and/or potential of cytotoxicity. Importantly, these metals and alloys materials are specifically appealing because they often possess high saturation magnetization which means they are easy to be separated, recycled and renewed through an external magnet. To overcome these drawbacks, a silica or carbon shell is introduced on the magnetic core to provide protection against oxidation, cytotoxicity and help to maintain long-term stability of the particles.^{26,27}

Thus, it is of great importance to develop a facile and effective method for the synthesis of metals and alloys based noble metal composite structures and exploring their SERS and reproducible performances. Unfortunately, there is few report on the synthesis and SERS performances of metals and alloys based silver composite microspheres up to date. In this paper, we report a new route to fabricate monodispersed NiCo@SiO₂@Ag (NSA) composite microspheres with an ideal reproducible nanosheet-assembled shell structure where strong SERS signals can be generated. The NSA composite microspheres were synthesized in three main steps based on a layer-by-layer procedure. Firstly, the magnetic NiCo alloys spheres as the core were prepared by a solution reaction at room temperature. Secondly, the NiCo alloys spheres were coated with a layer of silica by a modified Stöber method, which would disperse them well in water due to the hydrophilic properties of the silica shell; Thirdly, Ag seeds were introduced onto the surface of the silica shell for easier deposition of the subsequent silver shell, then the Ag nanosheet-assembled shell were successfully formed around the NiCo@SiO₂ microspheres. Raman experiments indicated that NSA composite microspheres with nanosheet-assembled shell structure showed the highest enhancement efficiency and high SERS sensitivity to p-aminothiophenol (p-ATP) and 4-mercaptobenzoic acid (MBA) molecules. And a low concentration of 10⁻⁷ M for both p-ATP and MBA could be detected. Such NSA composite microspheres exhibited good reproducibility across the entire area. Moreover, the superiority of the NSA composite microspheres in terms of their recoverability and recyclability was demonstrated through many successive cycles, under the external magnetic field.

2. Experimental Section

2.1. Sample Preparation

Synthesis of NSA composite microspheres. NSA composite microspheres were prepared according to previous method with minor modification.²³ 50 mg of the obtained NiCo@SiO₂ microspheres were firstly ultrasonically dispersed in 20 mL of absolute ethanol for 30 min, then mixed with [Ag(NH₃)₂]⁺ solution (2 mmol AgNO₃, 2 mL NH₃·H₂O, 20 mL ethanol) and stirred for 300 min. After separated by a magnet, 40 mL of ethanol containing 0.2 g of PVP was added, and the mixed solution was kept in a sealed flask at 70 °C under vigorous mechanical stirring and occasional sonication. After 3 h, NSA seed microspheres were obtained. Then, the above obtained NSA seed microspheres were redispersed in a mixed solution containing 2 mL AgNO₃ (0.5 M), 0.2 g citrate acid, and 40 mL deionized water under sonication and a mechanical stirrer, then

ascorbic acid solution (0.1 g, 10 mL) was added drop by drop in 15 minutes, and the reaction process was conducted under mechanical stirring and sonication. After the reaction was completed, the sample was washed by ethanol and deionized water repeatedly. Finally, the products were redispersed in 1 mL ethanol for further characterization.

2.2 Characterization

Field emission scanning electron microscope images were taken with a field emission scanning electron microscope (Quanta 200 FEG) operated at an accelerating voltage of 10.0 kV (ZYVEX, America). Transmission electron microscopy (TEM) and selected area electron diffraction (SAED) studies were performed with a JEOL-2010 microscope operated at an accelerating voltage of 200 kV with a tungsten filament. The phase and composition of the products were determined by a Rigaku D/Max- γ A rotating-anode X-ray diffractometer equipped with monochromatic high-intensity Cu-K α radiation ($\lambda = 1.54187 \text{ \AA}$). The magnetic characterizations of the samples were performed by using a superconducting quantum interference device (SQUID, Quantum Design MPMS-XL) magnetometer with fields of up to 20000 Oe. All measurements were performed at room temperature. The UV-Vis absorption spectra of the samples were recorded with a Shimadzu DUV-3700 spectrophotometer.

2.3 SERS measurement

P-ATP and MBA molecules were used as a Raman probe for the SERS measurements. For preparation of SERS substrates, the as-prepared NSA composite microspheres was immersed in 0.2 mL of p-ATP and MBA ethanol solutions respectively, then the samples were extracted using an external magnet and washed by ethanol and deionized water, and dried in air before the subsequent characterization. After the sample was carefully dropped onto clean glass slides, the substrates were measured using a Raman instrument. All SERS and Raman spectra were collected by a portable Raman instrument (*i*-Raman, B&W Tek Inc., USA) attached with a microscope (20 \times objective) and an optical fiber. The laser excitation wavelength was 1064 nm. During SERS measurements, the laser light was vertically projected onto the samples, and all SERS spectra were recorded by focusing the laser on the surface of the samples with a total accumulation time of 5 s. For each substrate, we took three SERS spectra in different positions of the substrate and then averaged them.

3. Results and Discussion

3.1. Morphology and structure of the sample

Preparation of NSA microspheres involves three main steps: Fabrication of magnetic NiCo particles as the core, coating silica onto the NiCo particles, and Ag nanosheet-assembling around the NiCo@SiO₂ microspheres. The typical SEM and TEM images in Fig. 1A-C show that uniform and monodispersed spherical particles with textured surface structure and a diameter of about 1.3 μm can be obtained using this method. Fig. 1D-F presents the images of uniform NiCo@SiO₂ microspheres with a core-shell structure. The silica shell is clearly visible as shown in Fig. 1F. Moreover, the shell thickness can be controlled by varying the concentration of TEOS and the reaction time.³⁰ The silica shell thickness of about 60 nm is controllable synthesized for the following assembling of silver shell. In this work, the silica shell

on the NiCo core not only effectively provides protection against oxidation and cytotoxicity, also improves the dispersibility of the magnetic microspheres. Fig. 1G-I shows images of Ag nanosheets assembled around NiCo@SiO₂ microspheres obtained under sonication and mechanical stirring conditions. It clearly reveals that large quantity and good uniformity of NSA microspheres with a mean particle size of about 1.7 μm are achieved using this approach (Fig. 1G), which is much bigger than the NiCo@SiO₂ microspheres, and the thickness of the Ag shell was estimated to be around 350 nm. It is also clear from Fig. 1H that as-obtained microspheres have a hierarchical surface structure which is assembled from many nanosheets with a thickness of about 20 nm. These nanosheets entangle with each other and form a wedge-shaped surface architecture. Rough edges are also seen around the composite microspheres in TEM image in Fig. 1I. Both the SEM and TEM images indicate that we have succeeded in controllable synthesis of spherical NSA core-shell micro/nanostructures.

A partial surface of hierarchical NSA microsphere is shown in Fig. 2A, which indicates the nanosheet self-assembled into spherical structure. The TEM image of a single NSA microsphere exhibits regions of varying contrast from the cores to the edges (Fig. 2B). The thin nanosheets are observed clearly in the edge of the microsphere. The HRTEM image (Fig. 2C) shows that the nanosheets are single-crystalline protrusions with interplanar spacing of about 0.245 nm. The SAED pattern (The inset in Fig. 2C) taken from this nanosheet reveals the hexagonal spot arrays which can be assigned to the [111] orientation of the FCC structure. The X-ray diffraction (XRD) patterns of the magnetic particles were displayed in Fig. 2D. The pattern (Fig. 2D-a) can be easily indexed to NiCo alloys. The diffraction peaks (Fig. 1D-b) of the NSA microspheres can be assigned to the (111), (200), and (220) planes of silver, respectively. The sharp and intense diffraction peaks of the NSA microspheres indicate high crystallinity of the particles. All the diffraction peaks of the products can be easily indexed to a cubic phase [space group Fm-3m] of silver (PDF No.04-0783). Besides, no obvious sharp diffraction peak corresponding to the SiO₂ is present, indicating that the SiO₂ coated around NiCo is amorphous. The increasing intensity of sharp diffraction peaks from the NSA microspheres shields the intensity of that from the NiCo, which indirectly proves the gradual growth of a silver shell around the NiCo@SiO₂ microspheres.

3.2. The evolution of the morphology and surface structure of the products

In the silver shell coating process, the silver seed modification has proved to be an efficient method for increasing the degree of surface coverage, since direct coating of a silver shell is rather difficult.³¹ In order to introduce Ag seeds into the composites, NiCo@SiO₂ microspheres were firstly immersed into an [Ag(NH₃)₂]⁺ solution for attraction and accumulation some silver ions on the silica surface. Subsequently, Ag seeds were grown onto the surface of NiCo@SiO₂ microspheres through reduction of Ag ions by PVP in ethanol (Fig.3A). These small silver nanoparticles served as nuclei sites for the subsequent growth of silver shells. The products synthesized at different reaction intervals were sampled and observed by SEM. During the silver shell growth, ascorbic acid (AA) was used as a reductant. After

1 reaction for 2 min, the original spherical NSA particles were
2 produced (Fig. 3B), revealing the initial silver seeds successfully
3 played the role of growing nuclei. With further extension of the
4 reaction time to 5 min, the products grew bigger with the addition
5 of AA and many densely nanosheets assembled on the surface of
6 the products can be observed (Fig. 3C). Further increase reaction
7 to 15 min, a complete Ag shell with rough edges on the surface of
8 NiCo@SiO₂ microspheres was formed (Fig. 3D). To obtain well-
9 dispersed NSA microspheres, we carried out the coating
10 experiments under the mechanical stirring and the sonication
11 technique, together with the dropwise addition of reducer.

12 Further experiments have revealed that the concentrations of
13 AgNO₃ also affect the final silver unit's morphology in our
14 experiments. Tuning the concentrations of AgNO₃ from 4 mL to
15 0.5 mL resulted in different surface feature of the products while
16 the general morphology of microsphere kept almost unchanged.
17 In these cases, the amount of citrate ions which is one kind of
18 morphology controlling reagent was kept constant. For example,
19 when the amount of AgNO₃ was increased to 4 mL, NSA
20 microsphere with thicker sheet (~ 80 nm) were yielded (Fig. 4A,
21 B). Decreasing the amount of AgNO₃ to 2 mL resulted in the
22 formation of thin nanosheet (20 nm) assembled NSA microsphere
23 as displayed in Fig. 4C, D. With the decrease of AgNO₃ to 1 mL,
24 the NiCo@SiO₂ microspheres were covered by short Ag
25 nanosheets (Fig. 4E, F). However, with further decrease of
26 AgNO₃ to 0.5 mL, sparsely and shorter Ag nanosheets assembled
27 NSA microspheres were produced as shown in Fig. 4G, H.
28 Because of the insufficient amount of AgNO₃, some parts of the
29 NiCo@SiO₂ surface were exposed outside. It is reported that
30 citrate ions not only serve as a capping agent to selectively bind
31 {111} facets, but also coordinate with Ag⁺ ions to form a variety
32 of complexes. The coordination effect can significantly reduce
33 the concentration of free Ag⁺ ions, thus slowing down the
34 reduction and enabling a kinetic control that favors nanoplate
35 formation.³² In our experiment, when large amount of AgNO₃
36 was adopted (for example, 4 mL), although a half of the silver
37 ions were proposed to be complexed with citrate ions in solution,
38 the concentration of free Ag⁺ ions increased largely. Then,
39 thermodynamic growth began to work, and the citrate ions
40 attached onto the {111} facets of silver units could not strongly
41 restrict the growth along the planar directions, thus the gradual
42 growth along the vertical directions led to the thicker nanosheet
43 seen in Fig. 4B. When the amount of AgNO₃ was decreased from
44 2 mL to 0.5 mL, citrate ions can completely stabilize the silver
45 ions, favoring the growth of nanosheets.

46 3.3. The magnetic response of the products

47 In the present work, the NSA composite microspheres could
48 simultaneously result in dual functions of both fast magnetic
49 response and local surface plasmon resonance. The magnetic
50 properties of the NiCo microspheres and NSA microspheres were
51 firstly characterized by a SQUID magnetometer at room
52 temperature. As shown in Fig. 5, the saturation magnetization
53 (Ms) value of NiCo microspheres and NSA microspheres is about
54 175 emu g⁻¹ and 43 emu g⁻¹, respectively. Such an excellent
55 magnetic property means that all of the prepared samples have
56 strong magnetic responsivity and can be separated easily from
57 solution with the help of an external magnetic force and for
58 recyclable application. The sharp decrease in magnetic saturation

60 can be explained in terms of the formation of the SiO₂ and Ag
61 shell surrounding the NiCo microspheres.³⁹ The magnified low
62 field curves also demonstrate the minor magnetic hysteresis loops
63 of the NiCo microspheres and NSA microspheres (the inset in Fig.
64 5). Moreover, the suspensions of both the NiCo microspheres and
65 NSA microspheres can be concentrated by an external magnet
66 within 30 s, leaving the aqueous solution transparent. When the
67 magnet was removed, the NSA microspheres were well dispersed
68 again in the aqueous solution by shaking, demonstrating that the
69 NSA microspheres have a good water-dispersive ability. When
70 these NSA microspheres used as Raman probes, analyte
71 molecules can be easily captured, magnetically concentrated, and
72 analyzed by SERS. Compared with pure silver microspheres, the
73 obtained magnetic-based hierarchical silver microspheres can be
74 separated from the sample solution, which shortened the
75 detecting time. Moreover, the rapid magnetic response ability
76 allows for the tracking or separation of such particles in a
77 magnetic gradient, paving the way for their sensitive and
78 recyclable detection of probe molecules.

79 3.4. Reproducible SERS substrate for high sensitive detection

80 It is well known that SERS spectroscopy is a unique
81 ultrasensitive technique that allows identification of the analytes.
82 The presence of cross-linked nanosheets assembled around
83 NiCo@SiO₂ microspheres is expected to significantly promote
84 local field enhancements on the surface of these particles that
85 might increase their SERS efficiency. Using a portable Raman
86 spectrometer, our SERS platform can identify p-ATP molecules.
87 Fig. 6A shows the SERS spectra of p-ATP adsorbed on NSA
88 microspheres substrates prepared at different reaction intervals.
89 The primary vibrations of p-ATP are confirmed according to our
90 previous work³³ and the literature.^{34,35} Two sets of bands were
91 observed on the SERS spectra of p-ATP on the surface of NSA
92 microspheres. One set is located at 1073 and 1587 cm⁻¹, which is
93 assigned to the a1 vibrational modes and the other set is located at
94 1136 and 1440 cm⁻¹, which is assigned to the b2 vibrational
95 modes. Obviously, the SERS intensity of the NSA seed
96 microspheres is the lowest, since only some tiny silver
97 nanoparticles were decorated on the surface of the NiCo@SiO₂
98 microspheres. The SERS intensity increases with the increase of
99 coating time and reaches a maximal value for 15 min. The reason
100 can be explained by the fact that the content of silver and the
101 number of silver nanosheets increase with prolonged coating time
102 which tends to form a large number of gaps or voids, providing
103 more active sites which afford potential high density 'hot spots'
104 to amplify the local electromagnetic fields as well as the Raman
105 signal. In addition, the SERS performance of products with
106 different morphologies shown in Fig. 4B-H was also investigated.
107 From Fig. 6B, it was observed that the roughened NSA
108 microspheres with cross-linked thin nanosheets (Fig. 4D) showed
109 the best SERS performance compared with the other shapes. This
110 result can be explained in two aspects. Firstly, the NSA
111 microspheres with cross-linked thin nanosheets (Fig. 4D) showed
112 the strongest plasmon peak at around 356 nm compared with the
113 other morphologies (shown in Fig. S2). When excited by
114 the irradiation, it could give rise to the strongest SERS
115 performance. Secondly, the reason was proposed to be the
116 different morphologies of the shell. It is widely believed that a
117 large enhancement could occur when a SERS active molecule is

positioned within the gap between two closely spaced metallic nanostructures.³⁹ The nano-scale cracks between two neighbouring nanosheets seen in Fig. 2A were also proposed to contribute to the SERS enhancement. And it was found the SERS signals weakened with decreasing density of nanosheets in Fig. 4H, due to the lower density of nanogaps providing fewer “hot spots” around the surface, thus resulting in inferior SERS signals. In this study, the sensitive properties of the NSA composite microspheres with maximum enhancement efficiency were selected as SERS substrates to detect representative SERS-active analytes such as p-ATP and MBA to test its effect. Fig. 7a demonstrates the results of SERS spectra of p-ATP with different concentrations adsorbed on the substrate from 10^{-4} M to 10^{-7} M. All the peaks observed in our SERS spectra can be attributed to p-ATP. The spectral intensities and resolutions are decreased with diluting the concentrations of the target molecules. It is found that additional p-ATP peaks still appeared at about 1073 and 1587 cm^{-1} at a low concentration of 10^{-7} M, which indicates that this SERS substrate is highly sensitive and promising for the detection of other target molecules. Hence, we examined the detection sensitivity of the as-obtained NSA composite microspheres for the detection of MBA molecules. The SERS spectra of MBA with different concentrations adsorbed on the NSA composite microspheres substrate are shown in Fig. 7b. The peaks from 800 to 1800 cm^{-1} are attributed to MBA signals; The two strong SERS peaks appearing at 1073 and 1582 cm^{-1} are assigned to ν_{8a} and ν_{12} aromatic ring vibrations, respectively; other weak bands around 1147 and 1181 cm^{-1} are attributed to the C–H deformation modes.³⁶ It is observed that two obvious SERS bands can still be detected in concentration ranges down to 10^{-7} M. This result indicated that NSA composite microspheres substrate also exhibited high detection sensitivity for MBA. In order to observe the enhancement intuitively and quantitatively, the SERS enhancement factor (EF)³⁷ was calculated as follows:

$$EF = \frac{I_{SERS} / N_{SERS}}{I_{bulk} / N_{bulk}}$$

where I_{SERS} and I_{bulk} denote the Raman scattering intensities from the p-ATP adsorbed on the surface of NSA composite microspheres and the solid p-ATP, respectively. N_{SERS} and N_{bulk} represent the numbers of the corresponding surface and solid molecules effectively excited by the laser beam, respectively. Based on the Raman intensity of the a1 vibrational modes at 1073 cm^{-1} and b2 vibrational modes at 1175 cm^{-1} (Fig. S1, ESI), the EF for a1 and b2 vibrational modes were calculated to be 3.0×10^5 and 4.8×10^5 , respectively, also showing good SERS activity of the NSA composite microspheres substrate. The uniformity of the NSA substrate was evaluated by collecting p-ATP (10^{-6} M) SERS spectra at 50 points that were randomly chosen on the substrate, and the relative standard deviations (RSD) of the intensities of the main vibrations were calculated, as shown in Fig. 8, respectively. Above all, the main Raman vibrations of p-ATP were obviously enhanced to a different extent at all spots of the NSA microspheres substrate, while the values of the RSD for the vibrations at 1073, 1136 and 1587 cm^{-1} are 11.27, 9.50, and 12.09 %, respectively, which are consistently less than 13 %, further indicating the uniformity of the substrate.^{38,39}

Based on the above analysis, it is clear that the Ag nanosheets-assembled NSA composite microspheres achieve high enhancement efficiency. Several factors are believed to simultaneously contribute to the Raman enhancement. The nanoscale gaps between neighbouring nanosheets on the surface of NSA provide high density hot spots, and the close approach of two entangled Ag nanosheets led to interaction of their localized surface plasmon resonances (LSPR), which is beneficial for SERS activity.^{40,41} When excited by the incident radiation, a collective surface plasmon is trapped between the neighboring nanoscale gaps, thus creating a huge local electric field at these gaps. Also their rough surface possesses a high specific surface area which favors the adsorption of probing molecules and the formation of high density and uniform gaps is easy for NSA to trap and capture probing molecules. Thus, it is not surprising that the NSA as SERS substrate performed with distinguished sensitivity and uniformity.

Finally, the recyclability of the substrate was examined through a series of experiments. A renewable substrate can be obtained for further detection if the target molecules adsorbed on the substrate can be fully cleaned by simple washing using water or ethanol. Fig. 9 shows the reversible SERS behavior of p-ATP and MBA adsorbed on the NSA microspheres over three cycles. By a simple magnetic separation, the substrate could be reused three times with no obvious decrease of the SERS intensity. The main reason for losing SERS signals is that the adsorbed target molecules on the substrate are washed away. Obviously, it is very simple and easy to realize the cleaning goal since the amount of target molecules adsorbing onto the substrate is low. After the substrate becomes clean, it can be repeatedly used several times. The SERS intensity does not show any obvious loss after three cycles for the detection of p-ATP or MBA. It is well-known that magnetic separation renders the recovery of material from a liquid reaction system much easier than the traditional separation procedures, such as filtration and centrifugation. The strong magnetic responsiveness of NSA microspheres (Fig. 5) is satisfied with the separation and collection in this study. This will provide an easy and efficient way to separate and recycle NSA microspheres from a suspension system with the help of an external magnetic force.

4. Conclusions

In summary, 3D hierarchically nanosheet-assembled NiCo@SiO₂@Ag composite microspheres have been successfully prepared by a layer-by-layer procedure at ambient temperature. The different surface structure of the silver shell can be obtained and controlled by adjusting the concentration of AgNO₃ and the reaction times. The gaps in or between cross-linked nanosheets in the shell of the microspheres is proposed to provide sufficient “hot spots” when they are used as a SERS substrate. The SERS measurement results, which are performed using a portable Raman instrument equipped with an optical fiber, show that NSA microspheres with nanosheet-assembled shell structure exhibit the highest enhancement efficiency and high SERS sensitivity to p-aminothiophenol (p-ATP) and 4-mercaptobenzoic acid (MBA) molecules. The resulting SERS substrate showed a highest analytical enhancement factor of $\sim 10^5$, a detection limit $\sim 10^{-7}$ M and a relative standard deviation

of the Raman peak maximum of $\sim 13\%$. In addition, the NSA microspheres with high saturation magnetization exhibit a quick response to an external magnetic field and show a good recoverability and recyclability. This research has great practical potential applications in rapid, on-site and reproducible trace detection of chemical, biological and hazardous materials in the field.

Acknowledgment. This work was supported by the National Natural Science Foundation of China (no. 61205150), the National Natural Science Foundation of China (no. 61378038), and the State Key Laboratories of Transducer Technology for financial support.

Notes and references

- 1 X. H. Xia, J. Zeng, B. McDearmon, Y. Q. Zheng, Q. G. Li and Y. N. Xia, *Angew. Chem., Int. Ed.*, **2011**, *50*, 12542–12546.
- 2 G. Sinha, L.E. Depero and I. Alessandri, *ACS Appl. Mater. Interfaces*, **2011**, *3*(7), 2557–2563.
- 3 Z. Liu, L. Cheng, L. Zhang, C. Jing, X. Shi, Z. B. Yang, Y. T. Long and J. X. Fang, *Nanoscale*, **2014**, *6*, 2567–2572.
- 4 M. Liu, Z. Y. Wang, S. F. Zong, H. Chen, D. Zhu, L. Wu, G. H. Hu and Y. P. Cui, *ACS Appl. Mater. Interfaces*, **2014**, *6* (10), 7371–7379.
- 5 J. F. Li, Y. F. Huang, Y. Ding, Z. L. Yang, S.B. Li, X. S. Zhou, F. R. Fan, W. Z. Z.Y. Zhou, D.Y. Wu, B. Ren, Z. L. Wang and Z. Q. Tian, *Nature*, **2010**, *464*, 392–395.
- 6 C. M. Girish, S. Iyer, K. Thankappan, V. V. Divya Rani, G. Siddaramana Gowd, D. Menon, S. Nair and M. Koyakutty, *J. Mater. Chem. B*, **2014**, *2*, 989–998.
- 7 X. M. Kong, Q. Yu, X. F. Zhang, X. Z. Du, H. Gong and H. Jiang, *J. Mater. Chem.*, **2012**, *22*, 7767–7774.
- 8 K. Ryu, A. J. Haes, H. Y. Park, S. Nah, J. Kim, H. Chung, M. Y. Yoon and S. H. Han, *J. Raman Spectrosc.*, **2010**, *41*, 121–124.
- 9 M. Li, S. K. Cushing, H. Y. Liang, S. Suri, D. L. Ma and N. Q. Wu, *Anal. Chem.*, **2013**, *85*, 2072–2078.
- 10 A. Chou, E. Jaatinen, R. Buividas, G. Seniutinas, S. Juodkazis, E. L. Izake and P. M. Fredericks, *Nanoscale*, **2012**, *4*, 7419–7424.
- 11 Y. Zhou, J. Chen, L. Zhang and L. B. Yang, *Eur. J. Inorg. Chem.*, **2012**, 3176–3182.
- 12 M. F. Zhang, A. W. Zhao, H. H. Sun, H. Y. Guo, D. P. Wang, D. Li, Z. B. Gan and W. Y. Tao, *J. Mater. Chem.*, **2011**, *21*, 18817–18824.
- 13 X. S. Wang, D. P. Yang, P. Huang, M. Li, C. Li, D. Chen and D. X. Cui, *Nanoscale*, **2012**, *4*, 7766–7772.
- 14 R. Li, C. Han and Q. W. Chen, *RSC Adv.*, **2013**, *3*, 11715–11722.
- 15 W. Moukarzel, J. Fitremann and J. Marty, *Nanoscale*, **2011**, *3*, 3285–3290.
- 16 H. Wei, B. Li, Y. Du, S. Dong and E. Wang, *Chem. Mater.*, **2007**, *19*, 2987–2993.
- 17 Y. Qin, Y. Song, N. Sun, N. Zhao, M. Li and L. Qi, *Chem. Mater.*, **2008**, *20*, 3965–3972.
- 18 J. F. Li, Y. F. Huang, Y. Ding and Z. L. Yang, *Nature*, **2010**, *464*, 392–395.
- 19 H. Wang and N. J. Halas, *Adv. Mater.*, **2008**, *20*, 820–825.
- 20 P. S. Kumar, I. Pastoriza-Santos, B. Rodriguez-Gonzalez, F. J. Garcia de Abajo and L. M. Liz-Marzan, *Nanotechnology*, **2008**, *19*, 1–5.
- 21 L. B. Yang, Z. Y. Bao, Y. C. Wu and J. H. Liu, *J. Raman Spectrosc.*, **2012**, *43*, 848–856.
- 22 Y. J. Ye, J. Chen, Q. Q. Ding, D. Y. Lin, R. L. Dong, L. B. Yang and J. H. Liu, *Nanoscale*, **2013**, *5*, 5887–5895.
- 23 Y. Q. Wang, K. Wang, B. F. Zou, T. Gao, X. L. Zhang, Z. L. Du and S. M. Zhou, *J. Mater. Chem. C*, **2013**, *1*, 2441–2447.
- 24 Z. B. Gan, A. W. Zhao, M. F. Zhang, W. Y. Tao, H. Y. Guo, Q. Gao, R. R. Mao, and E. H. Liu, *Dalton Trans.*, **2013**, *42*, 8597–8605.
- 25 N. T. T. Trang, T. T. Thuy, K. Higashimine, D. M. Mott, and S. Maenosono, *Plasmonics*, **2013**, *8*(2), 1177–1184.
- 26 B. L. Cushing, V. L. Kolesnichenko and C. J. O'Connor, *Chem. Rev.*, **2004**, *104*, 3893–3946.
- 27 L. X. Zhang, X. P. Sun, Y. H. Song, X. Jiang, S. J. Dong and E. A. Wang, *Langmuir*, **2006**, *22*, 2838–2843.
- 28 Stöber, W.; Fink, A.; Bohn, E. *J. Colloid Interface Sci.*, **1968**, *26*, 62–69.
- 29 M. F. Zhang, S. J. Shi, J. X. Meng, X. Q. Wang, H. Fan, Y. C. Zhu, X. Y. Wang and Y. T. Qian, *J. Phys. Chem. C*, **2008**, *112*, 2825–2830.
- 30 M. Ohmori, E. Matijevic, *J. Colloid Interface Sci.*, **1993**, *160*, 288–292.
- 31 J. H. Zhang, J. B. Liu, S. Z. Wang, P. Zhan, Z. L. Wang and N. B. Ming, *Adv. Funct. Mater.*, **2004**, *14*, 1089–1096.
- 32 J. Zeng, J. Tao, W. Y. Li, J. Grant, P. Wang, Y. M. Zhu and Y. N. Xia, *Chem.-Asian J.*, **2011**, *6*, 376–379.
- 33 M. F. Zhang, A. W. Zhao, D. Li, H. H. Sun, D. P. Wang, H. Y. Guo, Q. Gao, Z. B. Gan and W. Y. Tao, *RSC Adv.*, **2014**, *4*, 9205–9212.
- 34 Q. Zhou, G. Zhao, Y. W. Chao, Y. Li, Y. Wu, and J. W. Zheng, *J. Phys. Chem. C*, **2007**, *111*, 1951–1954.
- 35 Y. F. Huang, D. Y. Wu, H. P. Zhu, L. B. Zhao, G. K. Liu, B. Ren and Z. Q. Tian, *Phys. Chem. Chem. Phys.*, **2012**, *14*, 8485–8497.
- 36 A. Michota and J. Bukowska, *J. Raman Spectrosc.*, **2003**, *34*, 21–25.
- 37 C. J. Orendorff, A. Gole, T. K. Sau and C. J. Murphy, *Anal. Chem.*, **2005**, *77*, 3261–3266.
- 38 R. H. Que, M. W. Shao, S. J. Zhuo, C. Y. Wen, S. D. Wang and S. T. Lee, *Adv. Funct. Mater.*, **2011**, *21*, 3337–3343.
- 39 Q. Shao, R. H. Que, M. W. Shao, L. Cheng and S. T. Lee, *Adv. Funct. Mater.*, **2012**, *22*, 2067–2070.
- 40 P. J. Schuck, D. P. Fromm, A. Sundaramurthy, G. S. Kino and W. E. Moerner, *Phys. Rev. Lett.*, **2005**, *94*, 17402–17406.
- 41 V. Liberman, C. Yilmaz, T. M. Bloomstein, S. Somu, Y. Echegoyen, A. Busnaina, S. G. Cann, K. E. Krohn, M. F. Marchant and M. Rothschild, *Adv. Mater.*, **2010**, *22*, 4298–4302.

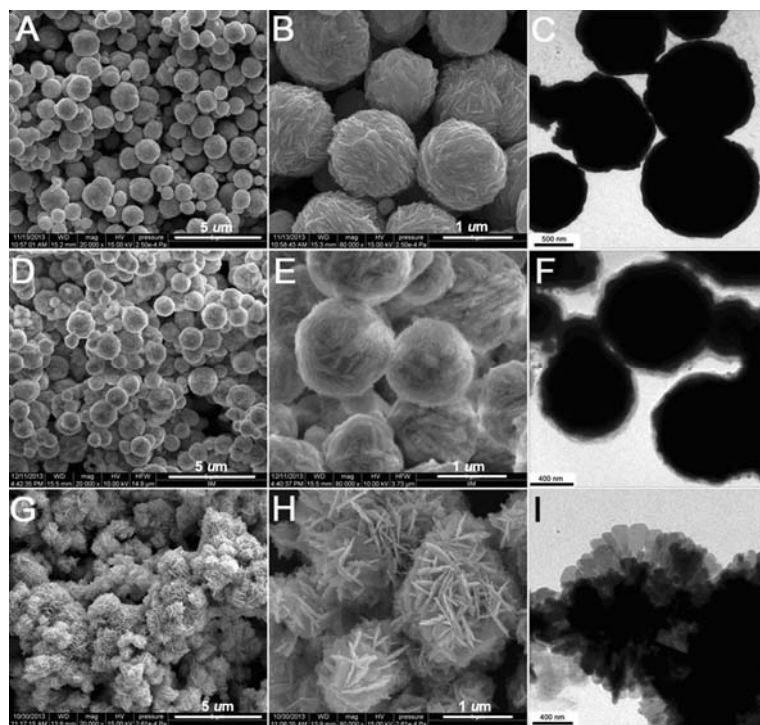


Fig. 1 SEM images of (A) NiCo, (D) NiCo@SiO₂, (G) NSA microspheres, and their corresponding magnified SEM images (B), (E), (H), and TEM image of (C), (F), (I), respectively.

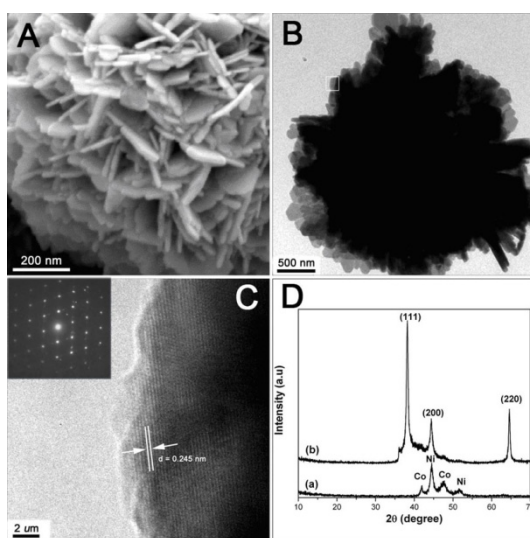


Fig. 2 Representative SEM image of (A) partial surface of NSA microsphere; (B) TEM image of a single NSA microsphere; (C) HRTEM image of a single Ag nanosheet and the SAED pattern (the inset) taken from the white square in (B); (D) XRD patterns of the as-prepared (a) NiCo particles and (b) NSA microsphere.

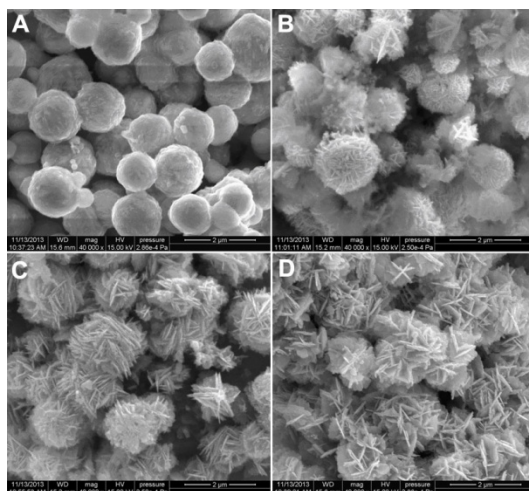


Fig. 3 The SEM images of NSA microspheres synthesized with AgNO_3 (2 mL) for different growing stages (a) seeding, (b) 2 min, (c) 5 min and (d) 15 min respectively.

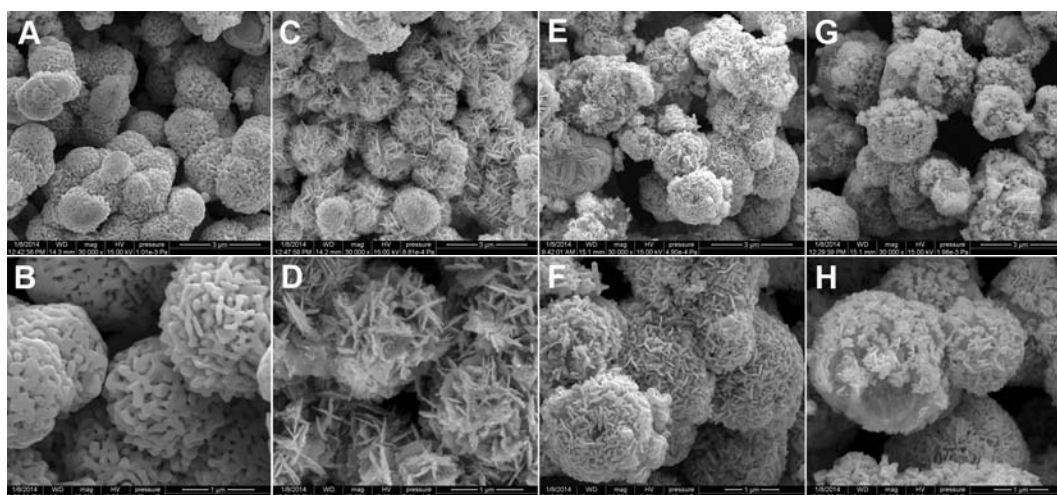


Fig. 4 The SEM images of NSA composite microspheres synthesized with different concentrations of AgNO_3 : (A) 4 mL, (C) 2 mL, (E) 1 mL and (G) 0.5 mL, and their corresponding magnified SEM images (B), (D), (F) and (H).

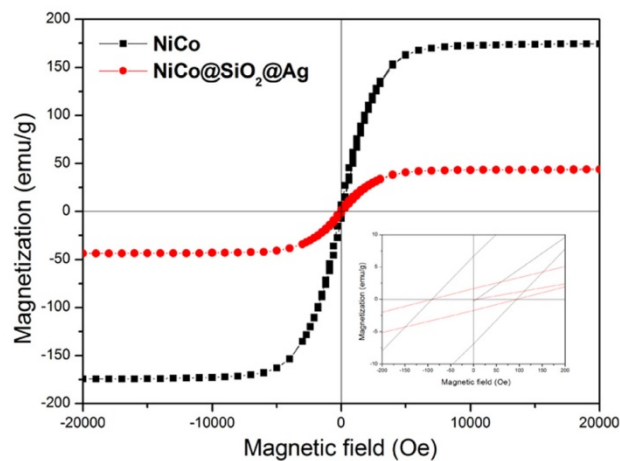


Fig. 5 Magnetic hysteresis loops of the NiCo microspheres and NSA composite microspheres. (The inset shows the magnified low field curves.)

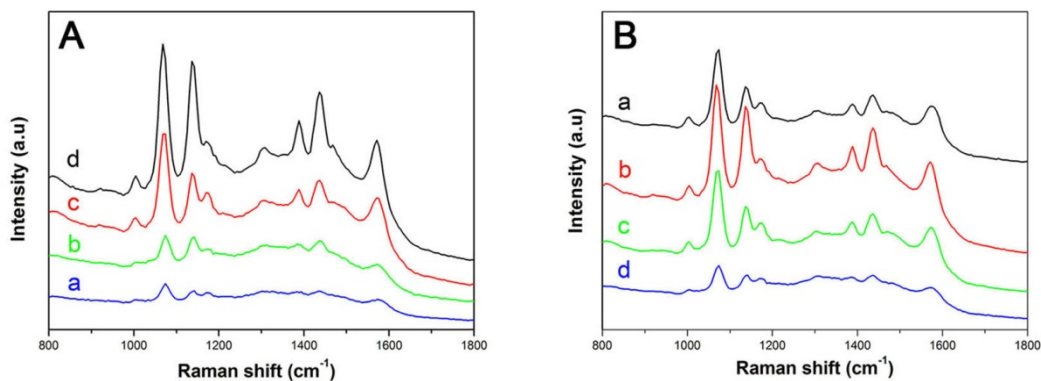


Fig. 6 SERS spectra of p-ATP (10^{-5} M) adsorbed on NSA composite microspheres (A) synthesized at different growing stages (a) seeding, (b) 2 min, (c) 5 min and (d) 15 min; (B) with different morphologies shown in (a) Fig. 4B, (b) Fig. 4D, (c) Fig. 4F, and (d) Fig. 4H.

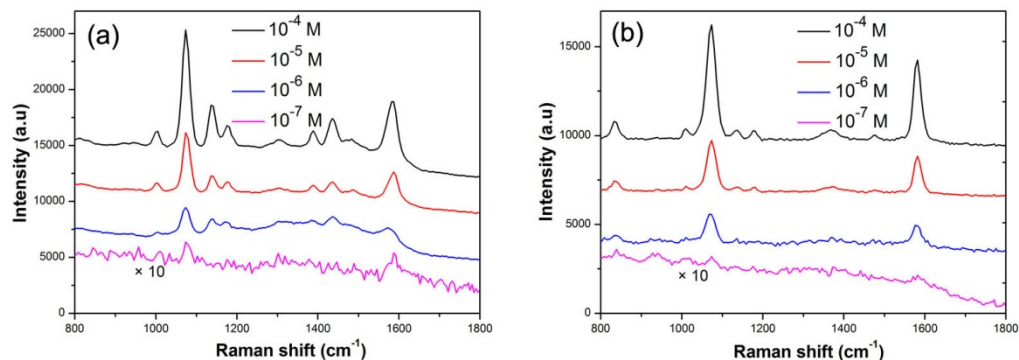


Fig. 7 SERS spectra obtained from different concentrations of (a) p-ATP and (b) MBA adsorbed on NSA composite microspheres.

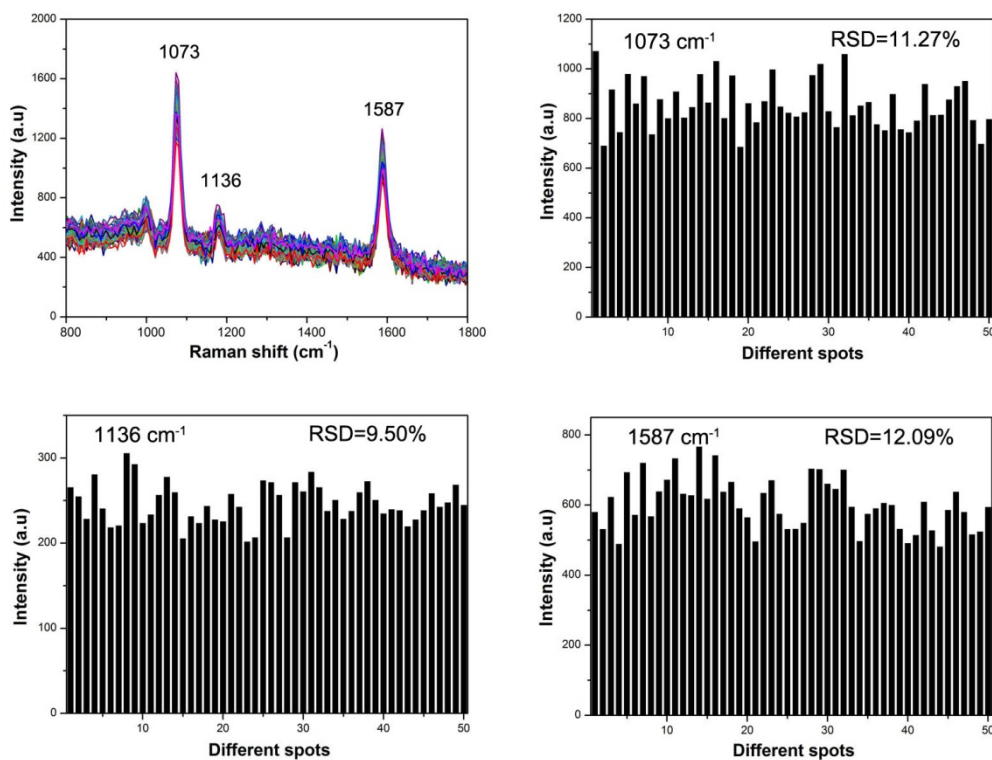


Fig. 8 A series of SERS spectra of p-ATP (10^{-6} M) molecules collected on 50 randomly selected spots of the NSA microspheres, and the intensities of the main Raman vibrations of p-ATP for SERS line-scan spectra collected on the NSA microspheres.

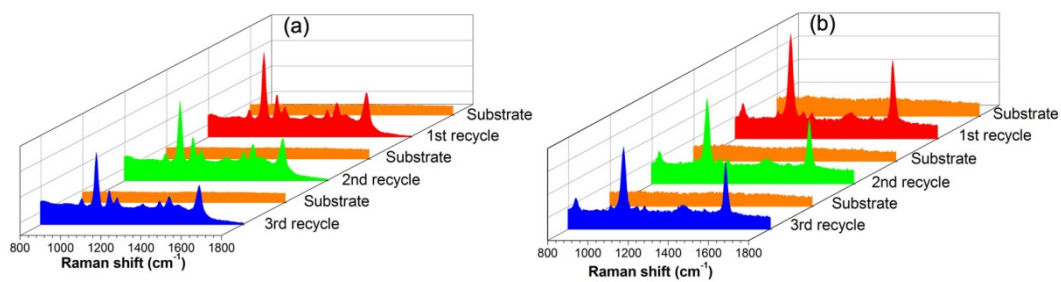


Fig. 9 Reversible SERS behavior of (a) 10^{-6} M p-ATP and (b) 10^{-6} M MBA on the NSA microspheres over three cycles.

Table of Contents

The hierarchically nanosheet-assembled NiCo@SiO₂@Ag core-shell microspheres exhibit a superior SERS performance, quick magnetic response, good recoverability and recyclability.

